

Preliminary Analysis of a Lazy Wave Riser Performance: Hydrostatic, Hydrodynamic, Modal, and Corrosion Assessments

¹Jonadab AhaotuObum, Elakpa Ada Augustine

¹Department of Mechanical Engineering, Faculty of Engineering, University of Port Harcourt, Port Harcourt, Rivers State, Nigeria

² Marine Engineering Department, Faculty of Engineering, Rivers State University, Nkpolu – Oruworukwo, Port Harcourt, Rivers State, Nigeria.

¹Corresponding Author

ABSTRACT

This paper presents an in-depth analysis of lazy wave risers, focusing on hydrostatic, hydrodynamic, modal, and corrosion behavior using a newly developed MATLAB-based tool, RiSat. The study addresses key challenges faced in offshore riser systems, particularly in high-pressure and high-flow environments, where riser design must account for complex load conditions. Through simulation, the hydrostatic forces, dynamic motion responses, and modal characteristics of the riser were calculated. In addition, corrosion analysis based on velocity and pressure variations was conducted, revealing exponential trends in corrosion rates. A detailed discussion of the results is provided, with comparisons to industry-standard tools such as OrcaFlex. The findings highlight critical insights into riser tension distribution, vibration frequencies, and failure modes, offering essential guidance for riser design in subsea environments.

Keywords: Marine Risers, Tension, Dynamic, analysis, structural, integrity, Corrosion,

Date of Submission: 04-02-2025 Date of acceptance: 14-02-2025

I. INTRODUCTION

The world's energy consumption has increased steadily since the 1950s. Fossil fuels (oil, natural gas, and coal) still amounts to 80% of the world's consumption even though a considerable number of initiatives and inventions in the area of renewable energy resources have decreased their use. The rapid rise in the price of crude oil prices during the 2000s is a response to the increasing demand for oil and gas. Of the fossil fuel consumed, almost 80% are oil and gas; therefore, the production of oil and gas is of major importance to the stability of the world's energy supply [22]. With the depletion of onshore and offshore shallow-water reserves, the exploration and production of oil in deep water has become a challenge to the offshore industry. Offshore exploration and production of oil and gas are advancing into deeper waters at an increasing pace. Offshore oil production from deep water has increased sharply since 1995, starting at approximately 20 million barrels of oil equivalent (MMBOE) per year from deep water (Mark, 2019). The subsea oil and gas exploration is not without it challenges. The subsea environment poses a host of challenges that the specialists who install rigs, flow routers, cables, risers and other critical structure must overcome to ensure that oil and gas flow efficiently from production assets. As the industry move to deeper waters, these challenges multiply in intensity (NS Energy, 2019).

A subsea production system consists of a subsea completed well, subsea Christmas tree and wellhead systems, subsea tie-in to flow line system, jumpers, umbilical and riser systems and subsea equipment to operate the well. The single of clustered well can be connected through the flow line to a fixed platform, FPSO (Floating Production storage and offloading) or onshore facilities. Due to the high pressures, potentially large temperature gradient and the harsh environment in the deep waters, the subsea systems and equipment are subjected to complex and critical load cases (oil and gas portal, 2015).

This work will be dealing with subsea risers, which is a system is essentially conductor pipes connecting floaters on the surface and the wellheads at the seabed and consists essentially of two kinds of risers, namely rigid risers and flexible risers.[21], with concentration on flexible riser.

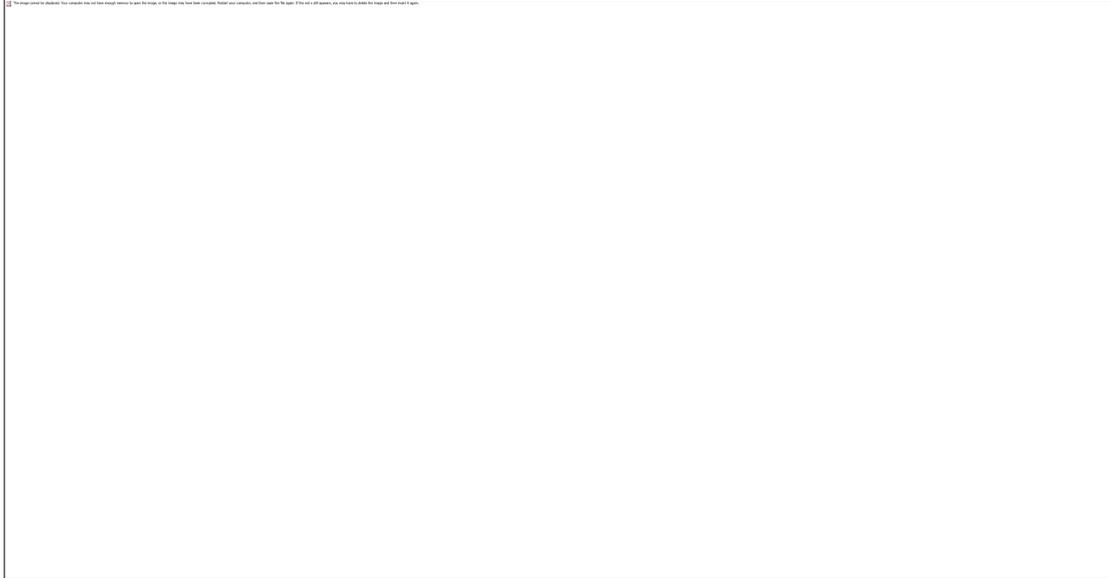


Figure 1: Flexible riser configurations [22]

Figure one shows the six major configuration of flexible riser and the lazy wave configuration is the major concern of this work. lazy waves are susceptible to configuration changes if the internal fluid density within the riser fluctuates over time [22] Various riser analysis tools are available for riser design, including: ABAQUS, ANSYS, etc. for General-purpose finite element programs, Flexcom, Orcaflex, Reflex, etc. for analysis, Shear7, VIVA, VIV ANA, CFD-based programs for Vortex-Induced Vibration (VIV) Analysis, and HARP, etc. for Coupled Motion Analysis Tools.[22]

While these tools are essential, the need to develop in-house codes arises to enhance the accuracy of data analysis and provide independence in conducting different analyses. Developing an in-house code allows for more tailored, flexible solutions that can better handle specific requirements, integrate unique datasets, and ensure a deeper alignment with the needs of the project. This independence supports greater customization, deeper insights, and the ability to innovate without being limited by external software capabilities.

Existing commercial tools for riser analysis, such as OrcaFlex, while powerful, often limit users from performing customized or locally tailored analyses due to software restrictions. This results in a dependency on external tools, limiting the ability to innovate and adapt analysis methods to meet specific local needs. There is a growing need for in-house analysis tools that provide engineers with the freedom to perform critical calculations—including tension, modal, bending, shear, and corrosion analysis—without the limitations imposed by commercial software. This thesis addresses this gap by developing a decision support system via a MATLAB-based graphical user interface (GUI), allowing for flexible, local analysis validated against industry standards.

Recent studies have demonstrated significant advancements in the development of graphical user interfaces (GUIs) in MATLAB for riser analysis. In a comprehensive work by Liu [5], the authors developed a MATLAB-based GUI for modeling and visualizing dynamic responses of deep-water risers. This interface simplifies user interactions, enabling non-expert users to efficiently set up simulations and analyze riser behavior under various environmental conditions. The integration of real-time data inputs and visualization in the tool is a notable achievement, facilitating faster decision-making in offshore operations.

Another significant contribution by Liu [5] focuses on a MATLAB GUI that incorporates both finite element methods and modal analysis for flexible riser dynamics. The study emphasizes the tool's capacity to handle complex riser configurations, including the calculation of stress, strain, and fatigue life across various scenarios. This tool's validation was carried out through comparisons with OrcaFlex results, demonstrating a high degree of accuracy in predicting riser performance under extreme conditions.

Furthermore, a GUI developed by Tian [18] focused on the fatigue and hydrodynamic analysis of risers, using MATLAB's computational flexibility to allow users to visualize vortex-induced vibrations and their impact on riser lifespan. The study's implementation of user-friendly modules for post-processing and result interpretation significantly enhanced its appeal for practical offshore engineering applications.

These papers collectively underscore the effectiveness of MATLAB GUIs in conducting detailed riser analyses, providing accessible platforms for engineers to simulate and analyze complex offshore systems.

II. MATERIAL AND METHODS

Model Overview

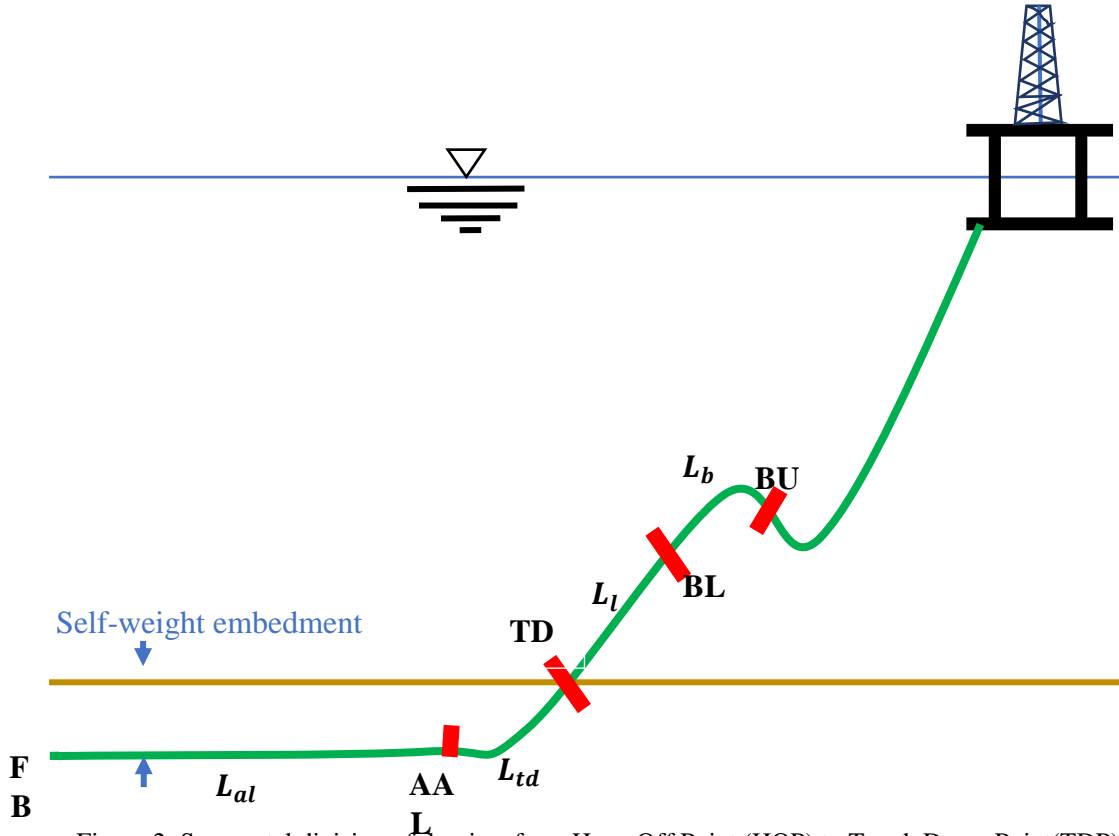


Figure 2: Segmental division of the riser from Hang Off Point (HOP) to Touch Down Point (TDP) (Trapper, 2020)

The structural analysis of the riser aims to determine its overall shape and configuration, specifically assessing the distance between the touch-down point (TDP) where the riser contacts the seabed and the hang-off point (HOP) where it is suspended. This analysis also involves evaluating the embedment depth into the seabed and the internal forces acting on the riser, such as bending, shear, and tension. The riser consists of several sections, beginning with the upper section (length L_u), which connects the HOP to the buoyancy section at point BU, typically exhibiting a sag bend.

The buoyancy section (length L_b) lies between points BU and BL, where buoyancy modules are installed. These modules generate an upward force, resulting in an arch bend in this section. Their effects are averaged over the section's length, represented as the equivalent submerged weight per unit length. Importantly, the addition of buoyancy modules does not significantly affect the riser's flexibility [14]. The lower section (length L_l) connects the buoyancy section at BL to the seabed at TDP, while the touch-down section (length L_{td}) extends from the TDP to the as-laid limit (ALL). The total length of the riser is defined as $L = L_u + L_b + L_l + L_{td} + L_{al}$, where $L_s = L_{td} + L_{al}$ represents the combined length of the touch-down and as-laid sections.

In this study, the touch-down section length L_{dt} is defined to ensure that the as-laid embedment occurs naturally at the endpoint (ALL). Thus, the as-laid section L_{al} is excluded from the minimal length of the suspended lazy wave riser (SLWR), noted as $L_{min} = L_u + L_b + L_l + L_{td}$, though it may extend beyond this minimum. The nature of the subsea unit connection at the riser's bottom end (e.g., well or flowline) may influence this condition, resulting in prescribed vertical displacement that is not solely due to self-weight. While these variations can be incorporated into the current model if necessary, their impact on the overall configuration of the SLWR is deemed negligible, allowing this paper to focus exclusively on the outlined conditions.

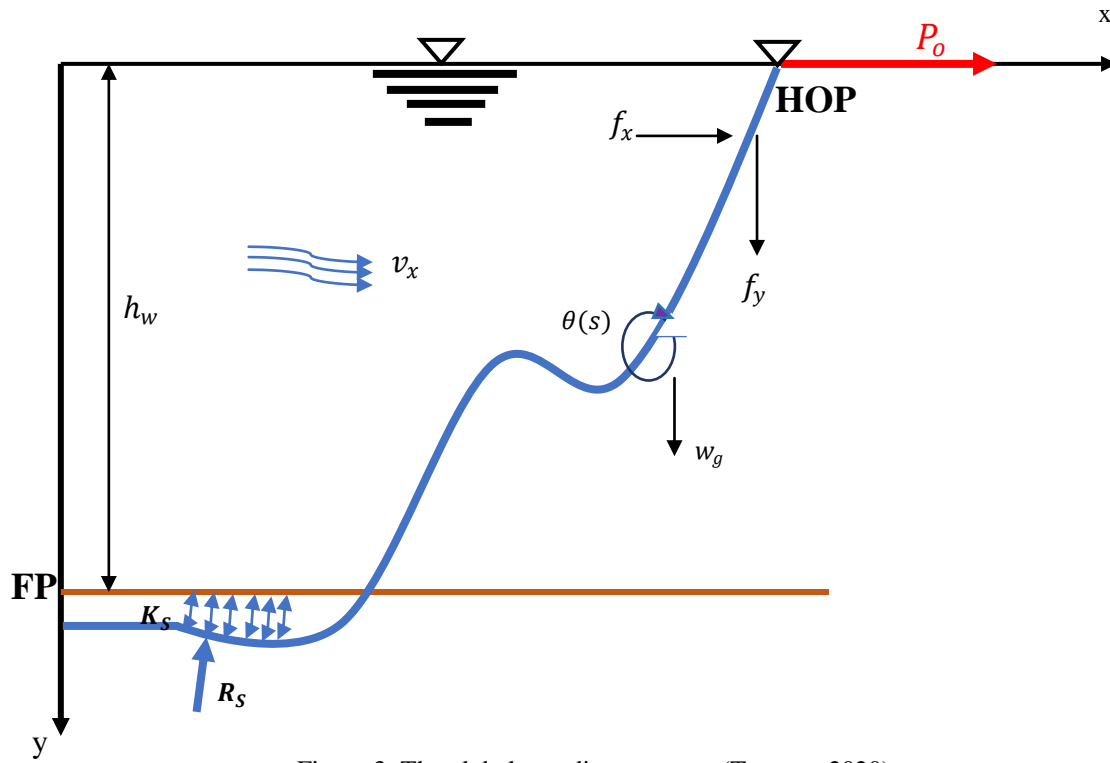


Figure 3: The global coordinate system (Trapper, 2020)

2.1 Mathematical Formulation for Riser Analysis

A comprehensive global analysis of the riser is performed to evaluate the overall load effects, focusing on its static configuration and extreme responses, including displacement, curvature, force, and moment due to environmental influences. The model is established in a global coordinate system (xy), with the origin located at the top left corner of the domain (see Fig. 3). The x -axis extends towards the host vessel (rightward), while the y -axis points downward toward the seabed. The elastic riser of length L is partially supported by the seabed, characterized by a linear stiffness K_s over a segment of length L_s at a depth h_w , with the remaining section suspended (Fig. 3).

The riser is subjected to several loads: a distributed submerged self-weight w_g acting along its entire length, a buoyancy load w_b along the buoyancy section L_b , and hydrodynamic forces f_x and f_y due to ocean currents moving at velocity v_x . Additionally, a horizontal tension point load P_o at the hang-off point (HOP), controlled by the host vessel, contributes to the overall load. The configuration of the riser is defined by $\theta(s)$, representing its local orientation along the arclength s (ranging from 0 to L) measured from a fixed point (FP). The boundary conditions for the configuration specify that at FP, the riser is constrained in the x -direction and prevented from rotating but can move freely in the y -direction, while at HOP, it is restrained in the y -direction but free to rotate and move in the x -direction.

The position of the riser is expressed in Cartesian coordinates x and y as follows:

$$x = \int_0^s \cos\theta(s') ds' \quad (1)$$

$$y = - \int_0^s \sin\theta(s') ds' \quad (2)$$

Equations (1) and (2) inherently satisfy the specified boundary conditions. By employing this coordinate system, the formulation naturally incorporates the boundary conditions in a straightforward manner, avoiding the complexity that would arise from using a different coordinate system, which might require additional methods such as Lagrange multipliers [1].

2.2 Minimum Total Potential Energy Principle in Riser Analysis

The principle of minimum total potential energy serves as a fundamental framework in solid and structural mechanics, enabling the derivation of governing equations through the principle of virtual displacements. This principle is central to classical variational methods, such as the Ritz method, commonly utilized in finite element models. In this study, the equilibrium configuration of the riser is formulated directly from this principle, which asserts that the stable equilibrium state corresponds to the geometric arrangement that minimizes the total potential energy, accounting for the forces and constraints acting on the system [16]; [19]. This energy approach simplifies the derivation process compared to traditional methods that require force and moment balance calculations on infinitesimal segments, ultimately producing similar results [20].

The total potential energy of the riser is composed of various components, including elastic strain energy and potential energy from applied forces. The expression for total potential energy is given by:

$$U_{total} = \frac{1}{2} \int_L EI k(s)^2 ds + \int_{L_s} k_s e(s)^2 ds - \int_L w_g y(s) ds - \int_{L_b} w_b y(s) ds - \int_L f_x x(s) ds - \int_L f_y y(s) ds - PoxL \quad (3)$$

The first term represents the bending elastic energy, while the second accounts for the elastic energy due to seabed deformation. The third and fourth terms address the potential energies associated with the riser's submerged self-weight and buoyancy modules, respectively, capturing the effects of distributed loads from ocean currents [15]. The methodology incorporates hydrodynamic loads using Morison's equations, which facilitate accurate quantification of fluid forces acting on the riser, thus providing a comprehensive analysis of its behavior under various loading conditions [8].

Once the angle θ is determined from the minimization of potential energy, further calculations of bending moments, shear forces, and tension along the riser can be executed using standard differential relationships, enhancing our understanding of the structural responses under varying environmental loads. The relevant equations for these calculations include:

$$M(s) = EI k(s) \quad (4)$$

$$S(s) = - \frac{dM(s)}{ds} \quad (5)$$

$$\frac{dT}{ds} = f_x \cos \theta(s) - (f_y + w(s)) \sin \theta(s) \quad (6)$$

where w_s encompasses the generalized gravity load, thereby providing a comprehensive framework for the analysis of riser stability and performance under operational conditions.

2.3 Finite Difference Discretization

In addressing the problem of riser dynamics, we employ the finite difference method, a straightforward numerical technique, while acknowledging that alternative methods, such as the finite element method, are also viable. The total potential energy of the riser, defined by Equation (6), is represented using discrete variables θ_i through a left Riemann sum:

$$U_{total} = \Delta s \sum_{i=1}^N \frac{1}{2} EI \left(\frac{\theta_{i+1} - \theta_i}{\Delta s} \right)^2 + \sum_{i=1}^{N+1} \frac{1}{2} k_{SB}^i (y_i - h_w)^2 - \sum_{i=1}^{N+1} w_i y_i - \sum_{i=1}^{N+1} f_x^i x_i - \int_L f_y y(s) ds - PoxL \quad (7)$$

Here, N represents the number of subintervals, and $\Delta s = \frac{L}{N}$ denotes the segment size. The seabed stiffness k_{sb}^i at node i is derived from the generalized equation, while the generalized gravity load at each node is defined as:

$$w_i = w(s) \Delta s \quad (8)$$

The nodal hydrodynamic loads f_x^i and f_y^i are calculated using the inertia and drag coefficients:

$$f_x^i = -f_l^i \sin \theta_i + f_d^i \cos \theta_i \quad (9)$$

$$f_y^i = f_1^i \cos\theta_i + f_d^i \sin\theta_i \quad (10)$$

To ensure static equilibrium, we optimize the total energy with respect to the discrete variables $\theta_1, \theta_2, \dots, \theta_{N+1}$ by solving:

$$\frac{\partial U_{total}(\theta_1, \dots, \theta_{N+1})}{\partial \theta} = 0 \quad \text{for } i = 2, \dots, N+1 \quad (11)$$

Substituting equations (4) and (5) into equation (11) yields a set of difference equations, leading to:

$$\begin{aligned} \frac{EI}{\Delta s}(-\theta_{i-1} + 2\theta_i - \theta_{i+1}) + \sum_{j=1}^i -k_{SB}^j [(-\sum_{k=j}^N \Delta s \sin\theta_k) - h_w] \Delta s \cos\theta_i - \\ \sum_{j=i+1}^{N+1} -f_x^j \Delta s \sin\theta_i - \sum_{j=1}^i -(f_y^j + w_j) \Delta s \cos\theta_i - P_0(-\Delta s \sin\theta) = 0 \quad \text{for } i = 2, \dots, N+1 \end{aligned} \quad (12)$$

This equation incorporates nodal forces and enables the calculation of riser configurations in static equilibrium, effectively capturing the mechanical behavior of the system under various loading conditions.

2.4 Numerical Implementation

To solve for θ , we can use the Levenberg-Marquardt algorithm [4]. We define the residual equation $f_i(\theta)$ as:

$$f_i(\theta) = \frac{EI}{\Delta s}(-\theta_{i-1} + 2\theta_i - \theta_{i+1}) + \Delta s \cos\theta_i \sum_{j=1}^N K^{\min(i,j)} \Delta s \sin\theta_j + h_w K_{SB}^i \Delta s \cos\theta_i + F_x^i \Delta s \sin\theta_i + F_y^i + W_i \Delta s \cos\theta_i + P_0 \Delta s \sin\theta_i \quad (13)$$

Then start with an initial guess of θ_i . The Jacobian matrix J is computed, and it is composed of partial derivatives of the residuals with respect to θ_i

$$J_{ij} = \frac{\partial f_i}{\partial \theta_j} \quad (14)$$

The residual vector is computed next,

$$f = [f_1(\theta), f_2(\theta), \dots, f_N(\theta)] \quad (15)$$

Note that element of the Jacobian matrix is the partial derivative of the residual with respect to each θ_j

Compute the gradient and Hessian approximation as follows

$$g = J^T f \quad (16)$$

$$H = J^T J \quad (17)$$

Modify the Hessian for stability (damping) as follows:

$$H' = H + \lambda I_{id} \quad (18)$$

Where λ is damping factor and I_{id} is the identity matrix.

Solve for the parameter update for $\Delta\theta$

$$\Delta\theta = -(H')^{-1} g \quad (19)$$

Then, update parameters

$$\theta_{new} = \theta_{old} + \Delta\theta \quad (20)$$

This is just one method that can be used in solving for the angle θ . Other methods such as the Marquardt's Algorithm, Coleman nonlinear minimization, Coleman Newton's reflective method, Dennis nonlinear least square,[7].

Since $\theta(s)$ has been defined, it is now possible to evaluate bending moments, shear forces and tension using the usual differential relations as given in equations (4), (5) and (6).

2.5 Beam Theory

The FEA method apply in this case is the Euler- Bernoulli's beam with end load, this is suitable Since risers are generally designed as slender, flexible structures. Generally, slender flexible designed structures are modeled as Euler–Bernoulli beams [10]. The model of the flexible three-dimensional Euler–Bernoulli beam with an end-load will be obtained by Hamilton's principle as follows:

$$\int_{t_1}^{t_2} \delta [E_k(t) - E_p(t) + W(t)] dt \quad (21)$$

where E_k is the kinetic energy, E_p is the potential energy, the virtual work is represented by W , δ represent the calculus of variations, t_1 and t_2 are constants, $t_2 > t_1$.

The kinetic energy E_k is expressed as

$$E_k = \frac{1}{2} m [(\dot{u})^2 + (\dot{v})^2 + (\dot{w})^2] + \frac{1}{2} \rho \int_0^1 [(\dot{u})^2 + (\dot{v})^2 + (\dot{w})^2] ds \quad (22)$$

where the first term represents the kinetic energy of the end-load, and the second term represents the kinetic energy of the Euler–Bernoulli beam [10]

The system potential energy is as given in equation (6).

The virtual work done by both the system inputs and the disturbances is

$$W(t) = U_u(t)u_1 + U_v(t)v_1 + U_w(t)w_1 + d_u(t)u_1 + d_v(t)v_1 + d_w(t)w_1 \quad (23)$$

Where \dot{u} , \dot{v} represents transverse acceleration, and \dot{w} represent longitudinal acceleration. u and v represent transverse displacements and w is the longitudinal velocity. U_u, U_v, U_w are boundary condition control input forces and d_u, d_v, d_w are corresponding boundary conditions input displacements.

2.6 Dynamic Response Solution

The dynamic behavior of the system can be described by the following equation of motion:

$$|M|\{\ddot{u}(t)\} + |C|\{\dot{u}(t)\} + |K_{stff}|\{u(t)\} = \{F(t)\} \quad [17] \quad (24)$$

Where

$|M|$ = the global mass matrix.

$|C|$ = the global damping matrix.

$|K_{stff}|$ = global stiffness matrix.

$|T|$ = the axial tension matrix

$\{u(t)\}$ = the nodal displacement vector

$\{\dot{u}(t)\}$ = the nodal velocity vector.

$\{\ddot{u}(t)\}$ = the nodal acceleration vector.

$\{F(t)\}$ = is the force vector, including the applied force $P_o(t)$

Using the Newmark-beta explicit scheme, specifying the parameters $\beta = 0$ and $\gamma = 1/2$ used to ensure the use of explicit method.

The Newmark-beta method computes the displacement $\{u(t + \Delta t)\}$ and velocity $\{\dot{u}(t + \Delta t)\}$ at the next time step using the following equations:

$$\{u(t + \Delta t)\} = \{u(t)\} + \Delta t \{\dot{u}(t)\} + \frac{\Delta t^2}{2} \{\ddot{u}(t)\} \quad (25)$$

$$\{\dot{u}(t + \Delta t)\} = \{\dot{u}(t)\} + \Delta t \{\ddot{u}(t)\} \quad (26)$$

The acceleration at the next time step $\{\ddot{u}(t + \Delta t)\}$ is calculated using the equation of motion:

$$\{\ddot{u}(t + \Delta t)\} = |M|^{-1} + (\{F(t + \Delta t)\} - |C|\{\dot{u}(t + \Delta t)\} - |K_{stiff}|\{u(t + \Delta t)\}) \quad (27)$$

Repeat the process for each time step. At each step, use the updated values of displacement $\{u(t + \Delta t)\}$, velocity $\{\dot{u}(t + \Delta t)\}$, and acceleration $\{\ddot{u}(t + \Delta t)\}$ to advance the solution in time.

2.7 Environmental Loads

Hydrodynamic forces of riser can also be considered from the approach of velocity potential [2]. Velocity potential can be applied to understand and predict the fluid flow around the riser, which significantly impacts the hydrodynamic forces acting on it.

For deep waters the velocity potential is given as

$$\phi(x, y, t) = \frac{A_m \omega}{K} e^{kz} \cos(Kx - \omega t) \quad (28)$$

Where:

A_m = is the wave amplitude

ω = is the angular frequency

k_n = wave number

x = horizontal position

z = is the vertical position (positive upward)

t = time

Velocity Field

The velocity field components are derived from the velocity potential ϕ

$$u = \frac{\partial \phi}{\partial x}; \quad v = \frac{\partial \phi}{\partial y}; \quad w = \frac{\partial \phi}{\partial z} \quad (29)$$

Calculating these:

x-component:

$$u = \frac{\partial \phi}{\partial x} = -A_w \omega e^{k_n z} \sin(k_n x - \omega t) \quad (30)$$

y-component:

$$v = \frac{\partial \phi}{\partial y} = 0 \quad (31)$$

z-component:

The axial velocity is assumed nonexistent. And then,

$$w = \frac{\partial \phi}{\partial z} = A_n \omega e^{k_n z} \cos(k_n x - \omega t) \quad (32)$$

Acceleration:

The acceleration components are obtained by differentiating the velocity components with respect to time:

$$\dot{u} = \frac{\partial u}{\partial t} = -A_w \omega^2 e^{k_n z} \cos(k_n x - \omega t) \quad (33)$$

$$\dot{v} = \frac{\partial v}{\partial t} = 0 \quad (34)$$

$$\dot{w} = \frac{\partial w}{\partial t} = -A_w \omega^2 e^{k_n z} \sin(k_n x - \omega t) \quad (35)$$

Displacement:

The displacement components are obtained by integrating the velocity components with respect to time. Assuming initial displacement at t=0 is zero:

$$\xi_x = \int U dt = -\frac{A_w}{k_n} e^{k_n z} \cos(k_n x - \omega t) \quad (36)$$

$$\xi_y = \int v dt = 0$$

$$\xi_z = \int w dt = \frac{A_w}{k_n} e^{k_n z} \sin(k_n x - \omega t) \quad (37)$$

2.7.1 Environmental Loads from Morrison's Equation

The hydrodynamic forces can be computed using Morrison's equation, which describes the force on a submerged structure due to waves and currents. The total hydrodynamic force F_H on the riser can be expressed as:

$$F_H = F_D + F_A = \frac{1}{2} \rho C_D A v^2 + \rho C_A A \dot{u} \quad (38)$$

Where:

F_H = total hydrodynamic force

F_D = drag force

F_A = added mass force

ρ = fluid density

C_D = drag coefficient

C_A = added mass coefficient

A = reference area of the riser

v = velocity of the fluid relative to the riser

\dot{u} = acceleration of the fluid

2.8 Eigenvalue Problem for Modal Analysis

In static structural analysis, modal analysis serves as a precursor to dynamic analysis by examining the inherent vibrational characteristics of a system under static conditions. Although static analysis typically focuses on loads that do not vary with time, understanding the natural frequencies and mode shapes is essential to prevent resonant conditions, where static loads could amplify dynamic effects.

For modal analysis, assume a harmonic response $\{u(t)\} = \{\phi(t)\}e^{i\omega t}$, leading to :

$$(|K_{stiff}| + |T| - \omega^2|M|) = 0 \quad (39)$$

Neglecting axial tension, the equation reduces to

$$(|K_{stiff}| - \omega^2|M|) = 0 \quad (40)$$

Where:

K_{stiff} = the global stiffness matrix,

M = the global mass matrix,

ω = the eigenvalue representing the square of the natural frequency,

ϕ = the eigenvector representing the mode shape.

Rearranging equation (40),

$$|K_{stiff}| \phi = \omega^2|M|\phi \quad (41)$$

This is a generalized eigenvalue problem. We need to solve for the eigenvalues ω^2 and the eigenvectors ϕ .

For more than two dimensional considerations, Risat tool, which applies iterative solution, is used. Just to illustrate in simple 2D case.

let's assume these matrices K_{stiff} and M , are given or have been computed from the system's physical properties as follows :

2.9 Corrosion Analysis

Corrosion rates

The rate of corrosion (or current density) is determined by the potential difference between the anode and the cathode and the resistance of the corrosion cell. The corrosion current is therefore:

$$I = \frac{V}{R} \quad (42)$$

The resistance of the cell may be as a result of electrical resistance or electrode polarization. The greater the resistance the lower the corrosion current and from Faraday's law the lower the mass loss. A high resistance within the corrosion cell is beneficial for control.

This resistance may result from one or more of the following factors:

- Resistance of the electrical connection between anode and cathode.
- Resistance of the electrolyte.
- High concentration of anode metal ions in solution.
- Reactant build-up at the cathode.
- Lack of reactants at the cathode.

The action of these resistances may be expressed in a polarization diagram. These diagrams plot potential difference versus current (or log current).

In general, the electrochemical and chemical rates of reactions due to either anodic or cathodic over potentials can be predicted using both Faraday's equation as follows:

$$R_F = \frac{i A_w j}{zF} \quad (\text{Nestor, 2004}) \quad (43)$$

Where i = applied current density (A/cm²)

$A_{w,j}$ = atomic weight of species j (g/mol)

z = oxidation state or valence number

f = Weight fraction of element

Now, dividing Faraday's rate of reaction, Eq., by the metal density defines the corrosion rate (rate of metal dissolution) as

$$C_{RG} = \frac{R_F}{\rho} \quad (44)$$

$$C_{RG} = \frac{i A_w}{zF\rho} = \frac{i_{corr} A_w}{zF\rho} \quad (\text{Nestor, 2004}) \quad (45)$$

The above equation is used to estimate the external corrosion of the system.

For the internal corrosion is taken to be the combined function of diffusion and erosion of multiphase fluid in a pipe wvchich is mathematically represented in mm/yr as the following:

$$C_{RI} = C_d + C_e \quad (46)$$

C_d = Corrosion by diffusion

C_e = Corrosion by erosion

Corrosion by diffusion refers to a specific type of corrosion process where the degradation of a material occurs primarily due to the movement (diffusion) of atoms or ions through a solid or liquid medium. This mechanism is particularly relevant in situations where there is a concentration gradient that drives the movement of species, such as metal ions, oxygen, or other reactants, which facilitates the corrosion process. The mathematical model for this type of corrosion is the diffusion model as follows:

$$C_d = \frac{1}{8} \pi \varphi L f R_e S C^{1/3} [12](47)$$

Where

L = length

φ = the turbulent diffusion coefficient for petroleum known as the Davis relation is given as:

$$\varphi = \frac{0.18\mu}{\rho} \left(\frac{\frac{d}{2} - h}{25dR_e^{\frac{8}{5}}} \right)^3 \quad (48)$$

h = Scale height

R_e = Reynold's Number , given by

$$R_e = \frac{\rho V d}{\mu}$$

f = Friction factor, given by

$$f = 0.00137 \left[1 + \left(\frac{20000h}{d} + \frac{10000}{R_e} \right)^{0.33} \right] \quad (49)$$

Sc = Schmidt number, given by

$$SC = \frac{\mu}{\varphi \rho}$$

Corrosion by erosion, also known as erosion-corrosion, is a degradation process that occurs when a material, typically a metal, is subjected to both chemical attack and mechanical wear. This phenomenon combines the effects of corrosion and erosion, leading to accelerated material loss compared to what would be observed if each process occurred independently. The mathematical model for erosion related corrosion is as follow s:

$$C_e = \frac{2V^3 \rho_m f}{P} \quad (50)$$

Where,

V = Velocity

ρ_m = Fluid density

f = Friction factor

P = Fluid pressure

III.RESULTS AND DISCUSSION

In the initial design phase of risers and pipes, selecting the right diameter and wall thickness is essential to optimize costs. This process is influenced by factors such as the operating philosophy, which covers transportation, pigging, corrosion management, and inspection, as well as well characteristics like pressure, temperature, flow rate, and fluid properties. Structural considerations, including burst, collapse, buckling, and installation challenges like vessel tensioning, must be accounted for, alongside construction factors such as manufacturability, welding, and tolerances [22]. Additionally, deep-water design requires assessing metocean conditions, vessel offsets, hydrodynamic loads, and soil interactions[15], while material selection focuses on strength, fracture toughness, fatigue resistance, and compatibility with sweet or sour environments [3]. These considerations guided the selection of parameters in Tables 1 and 2.

Table 1: Table of riser design data (Trapper,2020)

Parameters	Symbols	Values
Outer diameter of pipe (m)	D_o	0.2032
Pipe's wall thickness (m)	T	0.0191
Modulus of elasticity (N/m ²)	E	2.1 *E11
Density of steel (kg/m ³)	ρ_{st}	7850

Density of sea water (kg/m ³)	ρ_w		1030
Coefficient of drag		C_D	1.2
Inertia coefficient	C_T		0.024
Horizontal component of top tension (N)	P		200 000
Acceleration due to gravity (m/s ²)	G		9.81
Water depth (m)	D		2000
Upper section length (m)		L_U	1800
Buoyancy length (m)		L_b	600
Uplift loading ratio	$r_b = W_b/W_g$		2
Seabed stiffness (per unit length of the pipe) (N/m ²)	K_{sbs}		4000
Current surface velocity (m/s)	v_s		0
Finite difference subinterval size (m)		a	4

Table 2 : Table of riser corrosion data [9][12]

Parameter	Symbols	Value
Applied current (amps)	I_{cc}	101*E-6
Exposed area (m ²)	A_i	1
Oxidation number	Z	2
Riser length (m)	L_{tol}	2350
Faraday's Number (C/mol)	F	96485.34
Density of steel (kg/m ³)	ρ_{st} (or q_1)	7850
Pipe internal diameter (m)	D_i	0.165
Scale height (m)	H	0.01
Dynamic viscosity (Pa.s)	v_{vis}	0.00905
Fluid internal velocity (m/s ²)	v_{fl}	4
Internal pressure (N/m ²)	P_{int}	18400000
Density of internal fluid (crude oil)	ρ_{oil} (or q_2)	852.8

3.2 Static Results

These are results for static response, namely riser tension, Bending Moment and Shear force. Modal analysis result are also included. The explanation of the trends as well as its implications give engineers the requisite insight to deal with the various loads effect of the rider. The first graph is the riser Tension, the second one is the Bending moment, the next is shear force and the last on this section is Modal analysis.

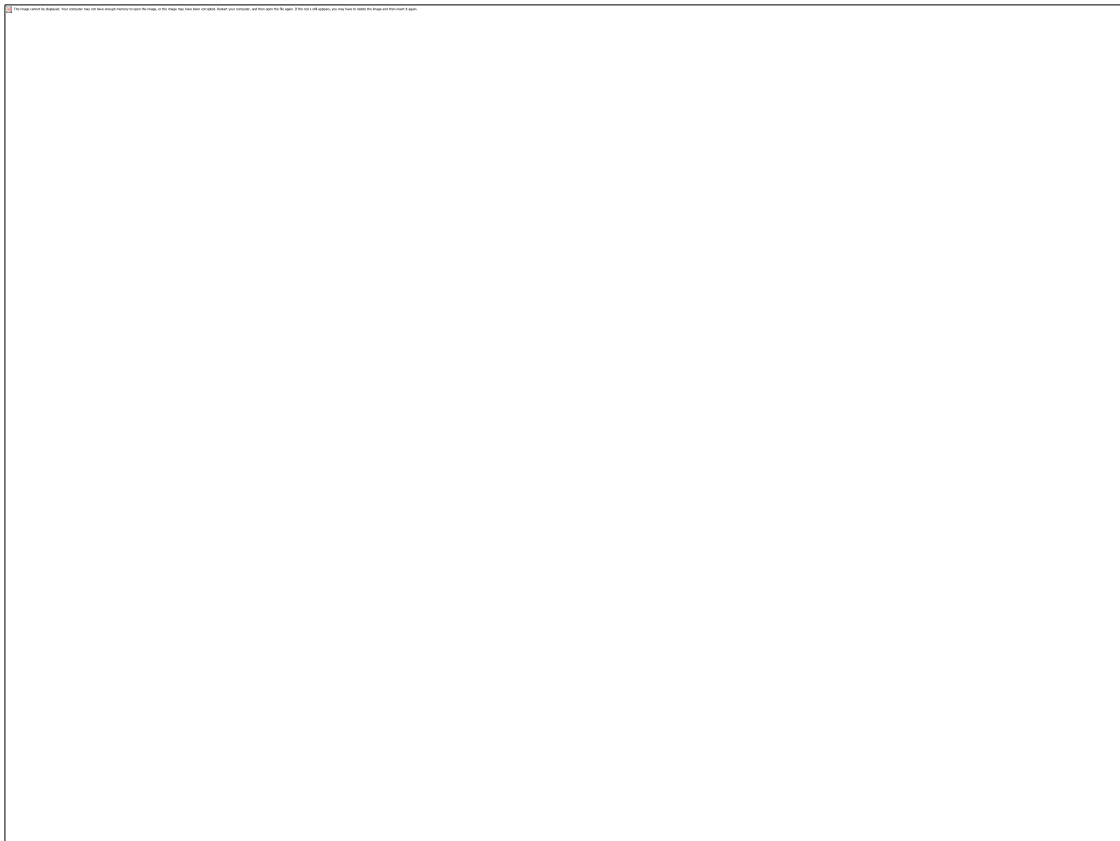


Figure 4: Graph of Tension Vs Riser Length

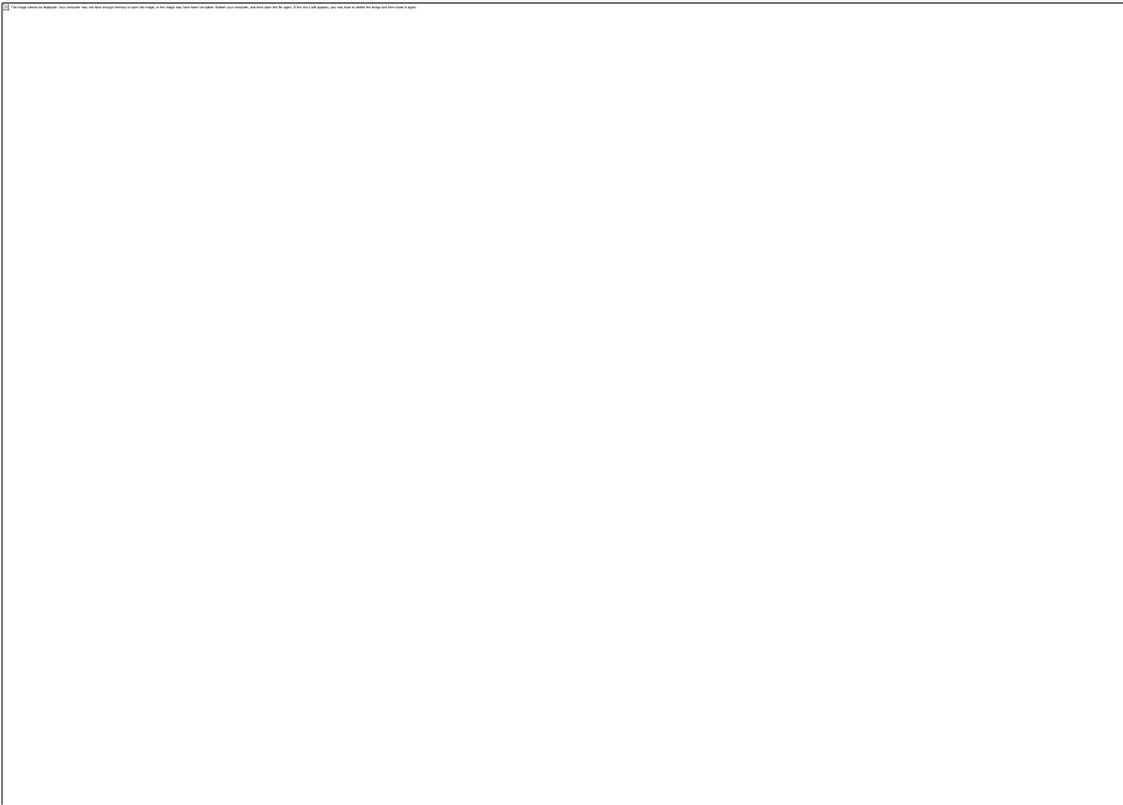


Figure 5: Graph of Bending moment Vs Riser Length

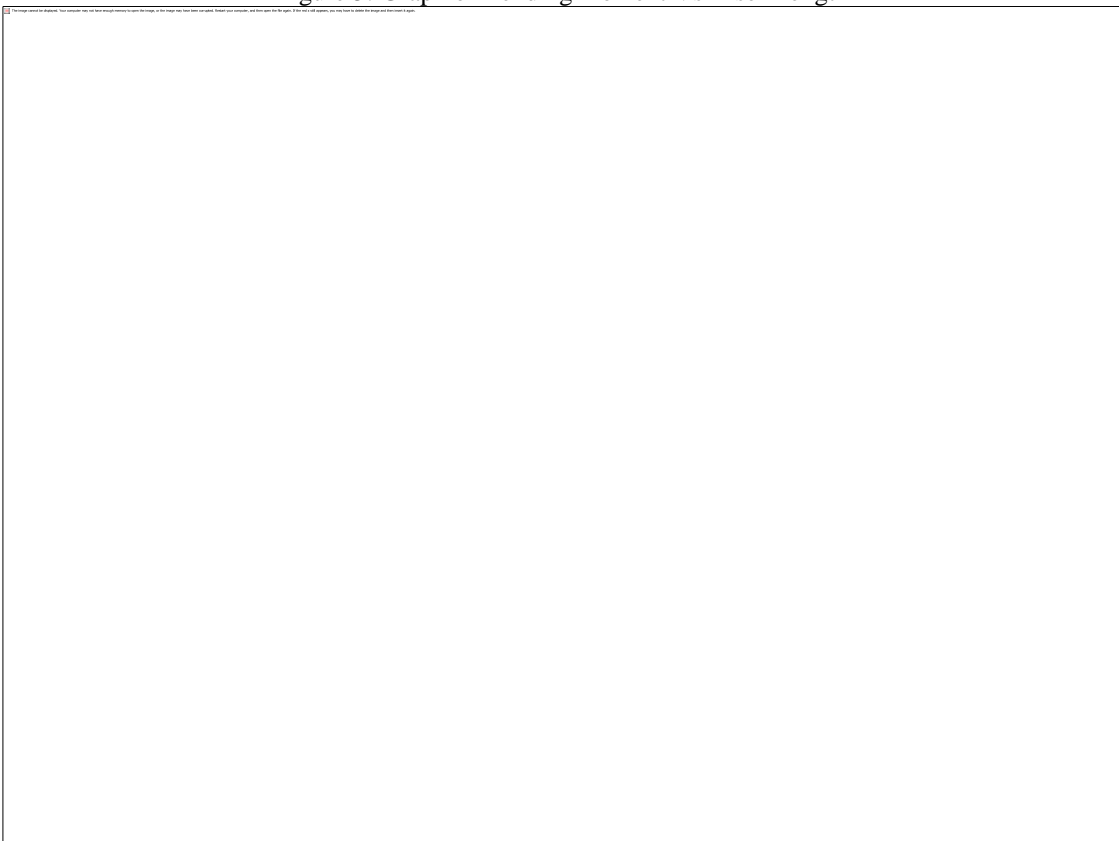
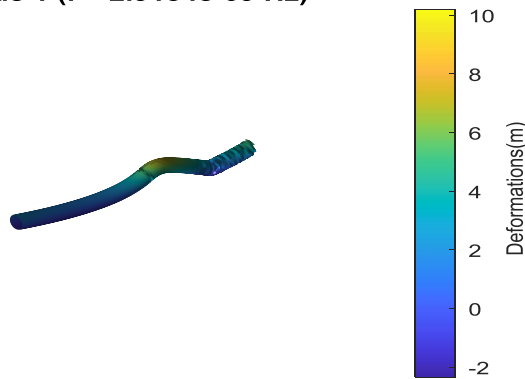
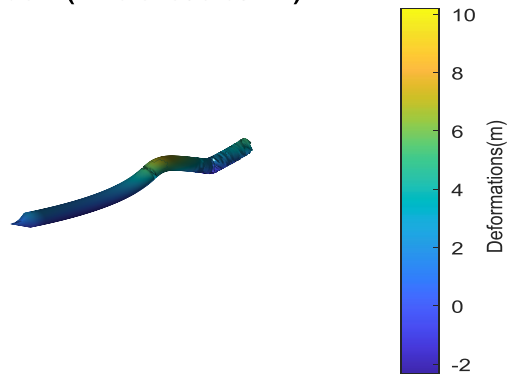


Figure 6: Graph of Shear force Vs Riser Length

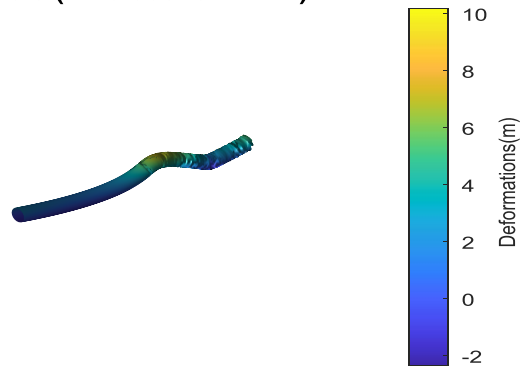
Mode 1 (f = 2.9134e-09 Hz)



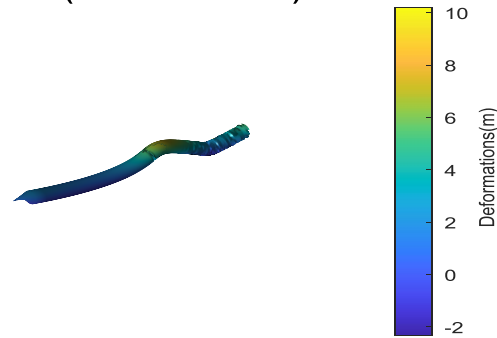
Mode 2 (f = 3.3139e-09 Hz)



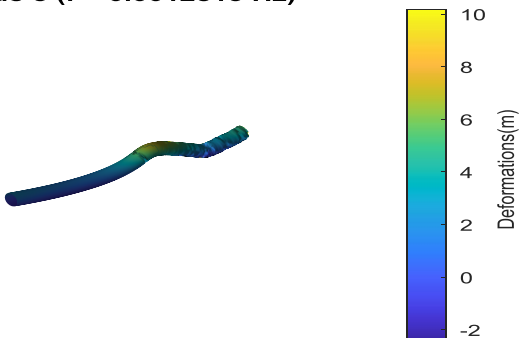
Mode 3 (f = 0.00023711 Hz)



Mode 4 (f = 0.00065361 Hz)



Mode 5 (f = 0.0012813 Hz)



Mode 6 (f = 0.0021181 Hz)

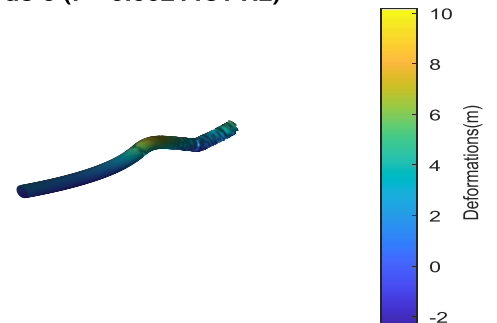


Figure 7: Modal Analysis

3.2.1 Static Results Discussions

The static response of the riser was analyzed, focusing on riser tension, bending moment, shear force, and modal analysis. These results provide crucial insights for engineers to manage various load effects on the riser. As seen in figure 4, the tension decreases along the riser length, with the maximum tension at the top (0 m), where the riser supports its full weight. As you move downward, tension steadily declines, reaching its lowest at the bottom (3000 m) where no further weight is supported. From figure 5 bending moment fluctuates significantly near the top, indicating dynamic forces like currents or wave loads, but stabilizes after 500 m along the riser. This stabilization suggests a more even distribution of forces further down, as the riser settles into a stable shape. Figure 7 depicts a sharp spike in shear force occurs near the top, driven by external forces and tension. Beyond the peak at 500 m, shear force stabilizes, indicating minimal shear forces in the lower sections of the riser.

The modal analysis of the riser model reveals six natural vibration modes, with frequencies ranging from extremely low values (2.9134e-09 Hz for Mode 1) to 0.0021181 Hz for Mode 6. Each mode indicates the riser's dynamic response under external loading, with progressively more complex deformation patterns as the mode number increases.

- **Mode 1 and 2:** These are nearly rigid-body motions, with minimal oscillation and deformation.
- **Mode 3 to 6:** Increasing frequency and deformation complexity, involving bending and twisting, with localized regions of high deformation (yellow) as shown in the color-coded legend.

In conclusion, the static and modal analyses show the riser experiences decreasing tension and shear forces along its length, while modal analysis reveals low-frequency oscillations with increasing deformation in higher modes. This analysis is essential for understanding the dynamic behavior of the riser in an offshore environment, informing engineers about potential fatigue risks and failure points over time.

3.3 Dynamic Results

The velocity potential approach provides a robust framework for analyzing the dynamic forces on risers by detailing fluid velocities, accelerations, and displacements. This method is instrumental in designing risers capable of withstanding the challenging conditions of deep-water environments. The following analysis details the dynamic characteristics of the riser at the top, middle, and bottom sections concerning displacement, velocity, and acceleration.

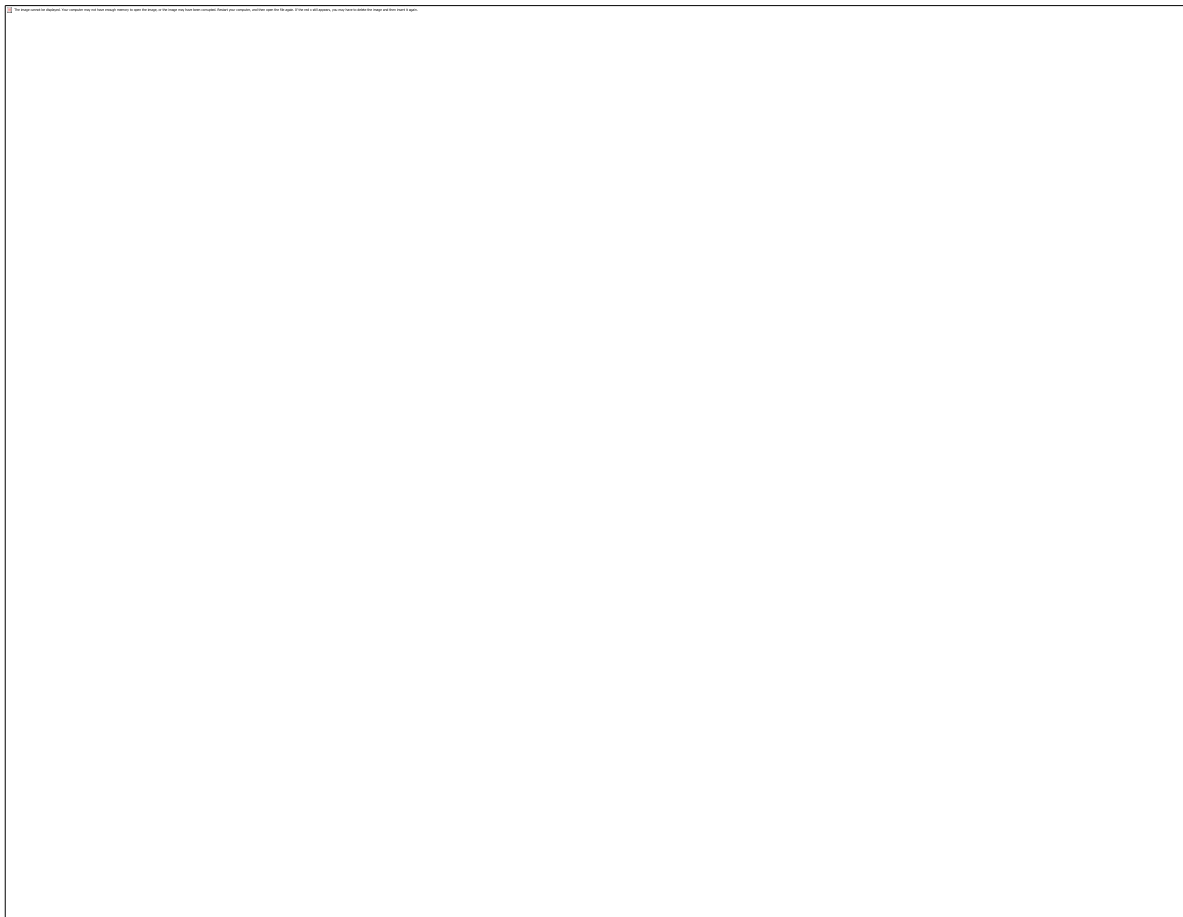


Figure 8 : Displacement Vs Time graph (Top)

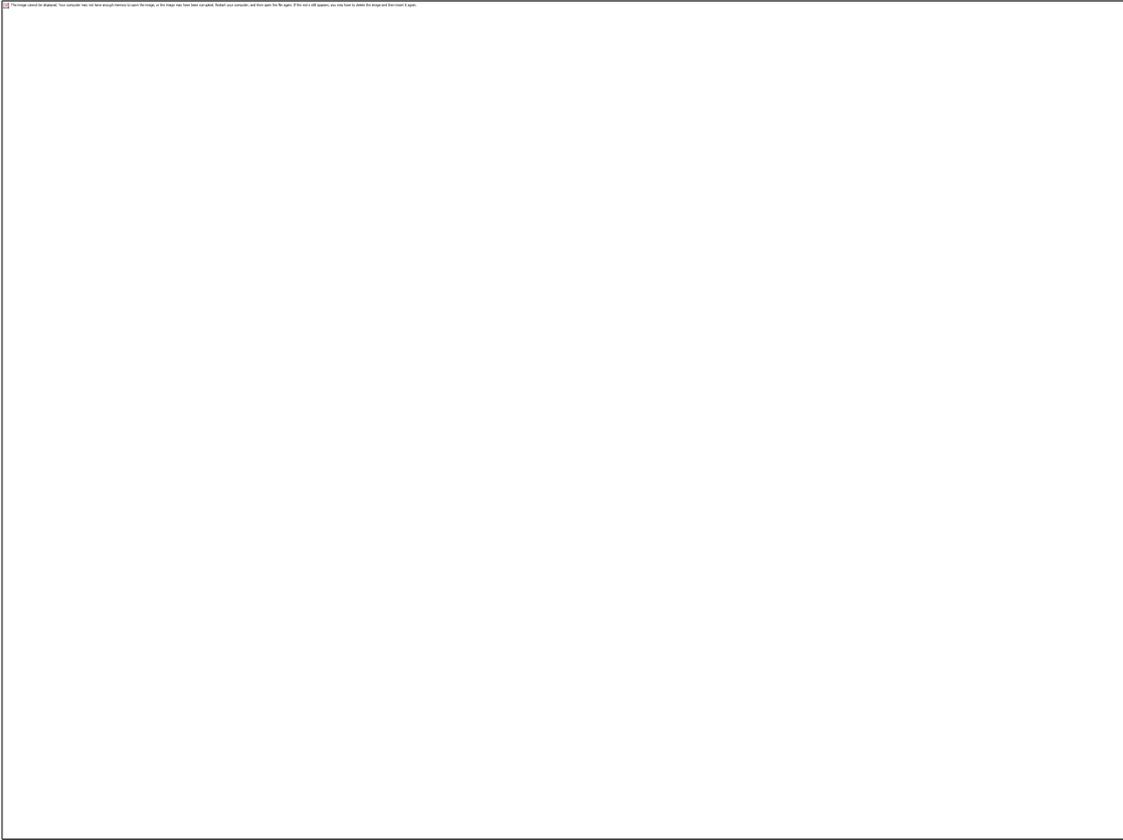


Figure 8: Velocity vs Time (Top)

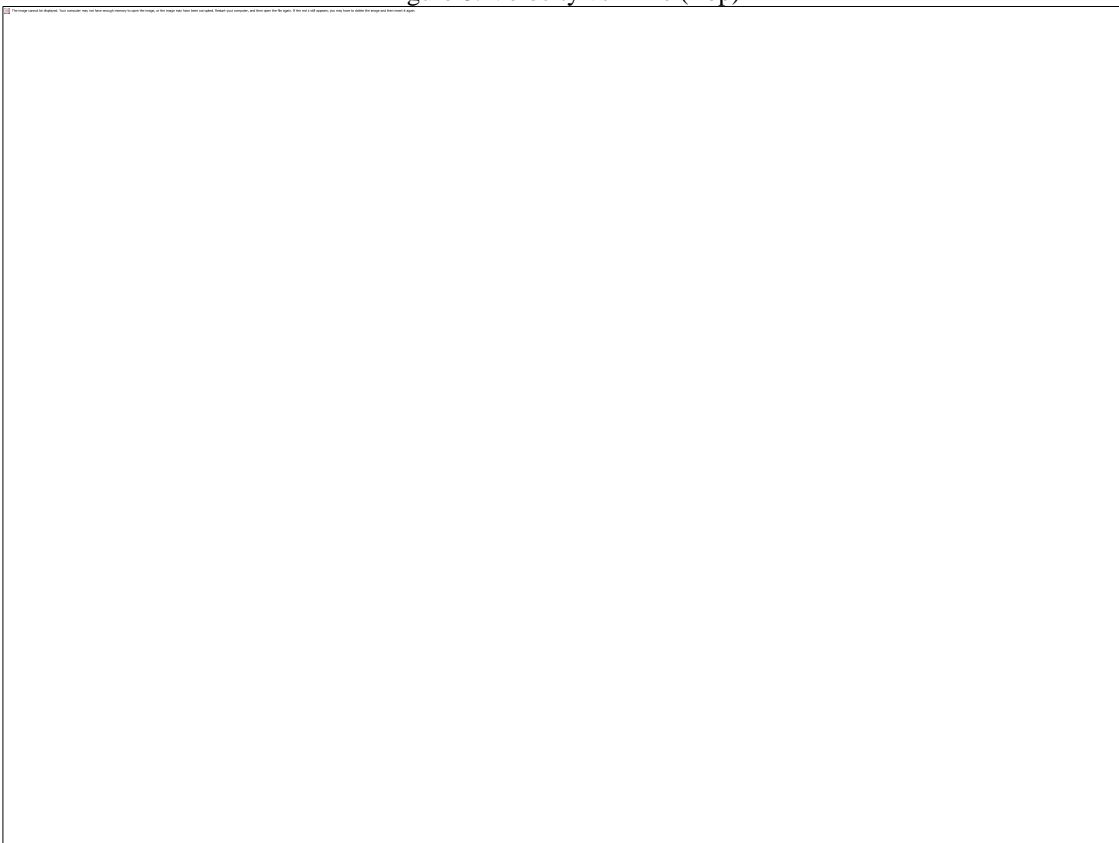


Figure 9: Acceleration vs Time (Top)

3.3.1 Top Section Dynamics: The displacement graph for the top of the riser shows a notable trend over time. Initially, from $t=0$ to approximately $t=1s$, the displacement starts near zero and experiences a sharp rise to a positive peak, indicating a rapid outward motion. Following this initial spike, the system undergoes damped oscillations between $t=1s$ and $t=6s$, with peaks decreasing in magnitude over time. The largest peak occurs around $t=1.5s$, and each subsequent peak diminishes, illustrating the loss of energy in the system due to damping effects, such as friction or resistance. As time progresses, particularly from $t=6s$ to $t=10s$, the oscillations decrease further, approaching zero displacement and signaling a return to an equilibrium or rest position. The velocity graph for the top section mirrors this trend, beginning at near-zero and rapidly increasing to a positive peak around one second. After this point, the velocity oscillates between positive and negative values, reflecting alternating upward and downward motions influenced by dynamic loading. By the end of the observation period, the velocity stabilizes, approaching zero, suggesting that the top of the riser experiences significant dynamic forces but ultimately moves toward equilibrium. The acceleration profile at the top reveals a similar pattern, with an initial spike indicating a rapid change in motion due to external forces. This is followed by large amplitude oscillations, reflecting the riser's dynamic interaction with its environment. Over time, the amplitude of these oscillations diminishes, indicating that the riser is dissipating energy and stabilizing.

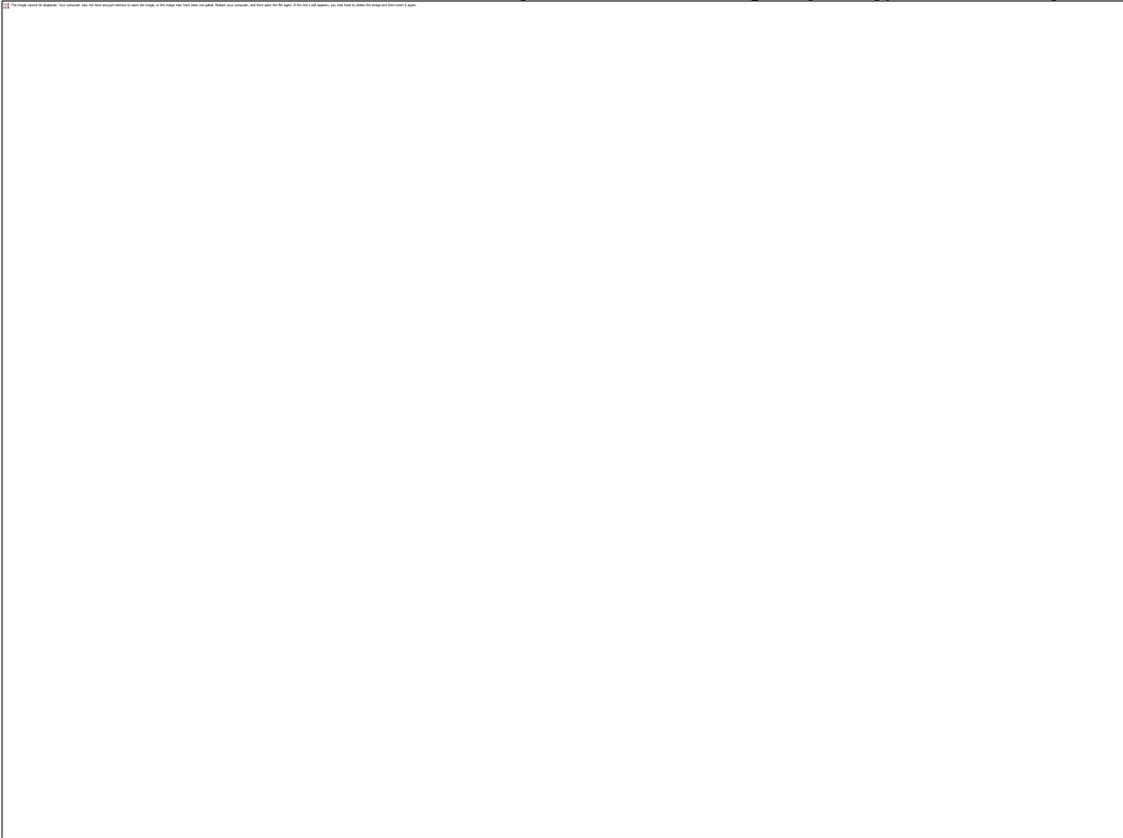


Figure 10: Displacement Vs Time (Mid-point)

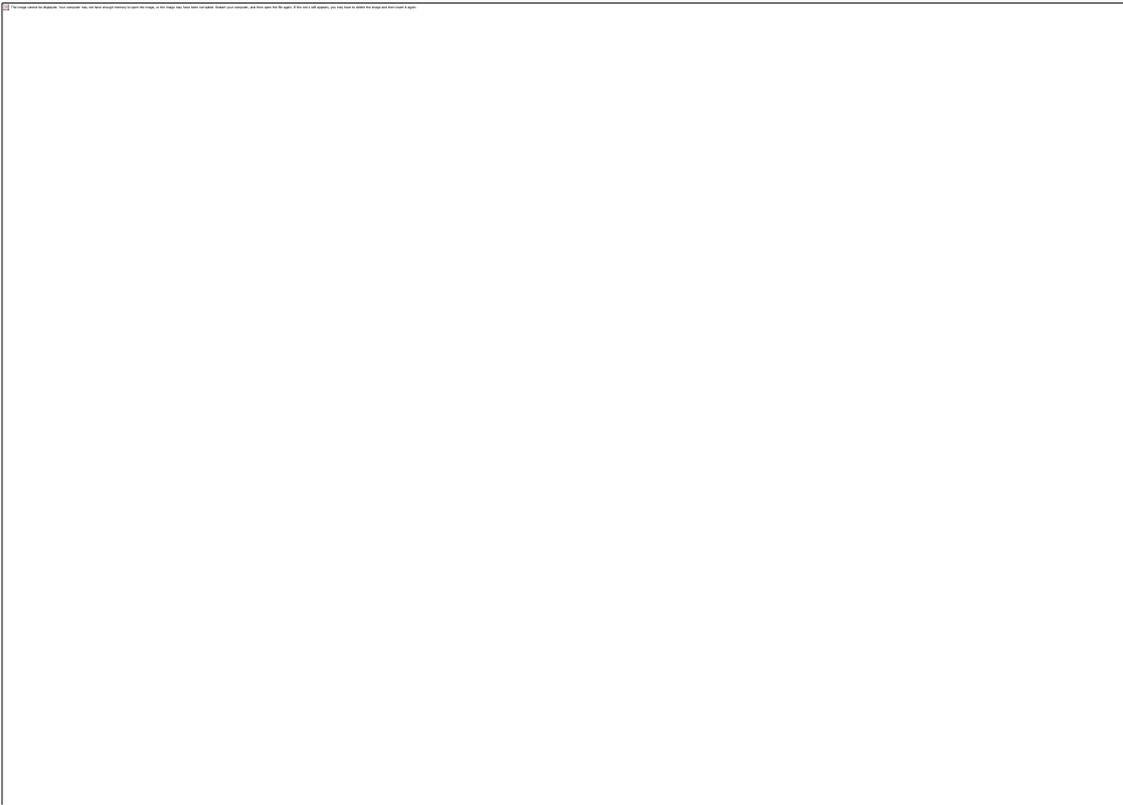


Figure 11: velocity vs Time (Middle)

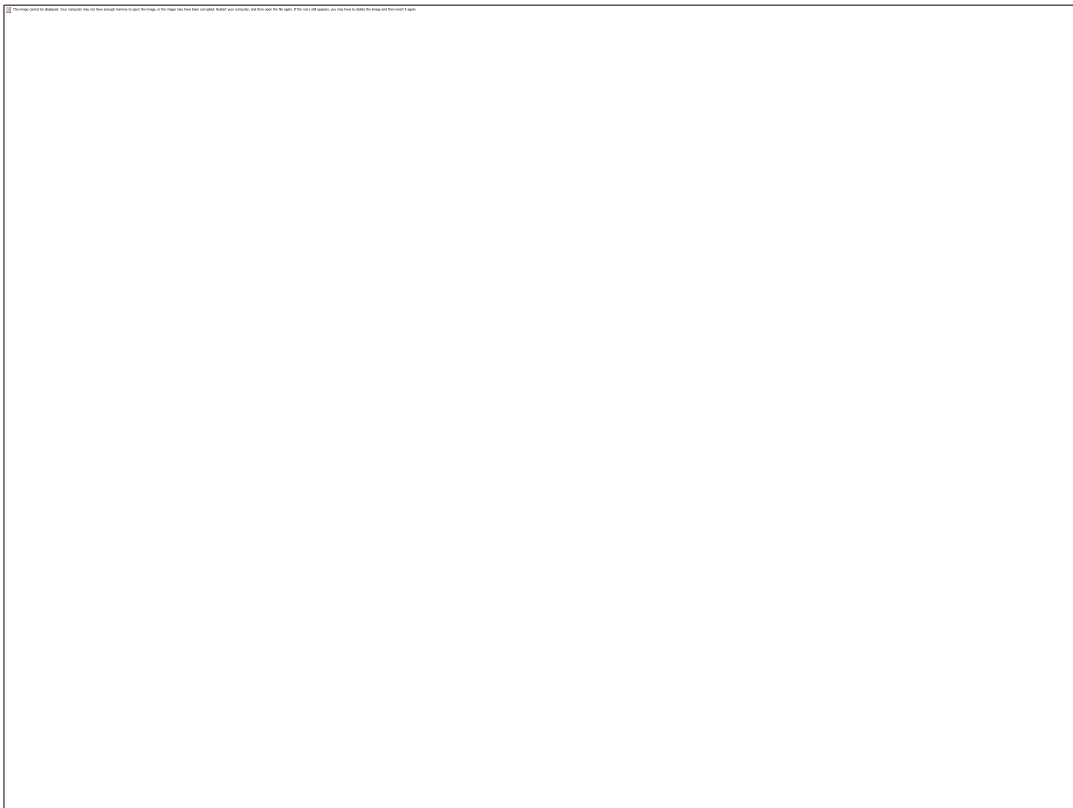


Figure 12: Acceleration vs Time (Middle)

3.3.2 Middle Section Dynamics: In contrast, the middle section of the riser exhibits a different dynamic behavior. The displacement graph indicates that the system begins slightly below zero, showcasing an initial inward motion that dips to a negative peak at around one second. Following this initial dip, the displacement shows a more controlled oscillatory behavior, less pronounced than that of the top section. By around $t=5s$, the displacement starts to rise steadily, suggesting that the middle of the riser stabilizes into a consistent outward motion with minimal oscillation. This behavior indicates that the effects of external forces are less significant at this point in the riser, leading to a more stable overall motion. The velocity profile reflects a sharp initial peak followed by damped oscillations, gradually smoothing out to a near-constant value by $t=10s$. This trend reinforces the idea that the middle section of the riser experiences less oscillatory motion compared to the top, emphasizing its role in maintaining stability under dynamic conditions. The acceleration graph for the middle section shows an initial peak followed by decreasing oscillations, indicating a damped response typical of dynamic systems. As time progresses, the oscillations decay towards zero acceleration, which is consistent with the behavior expected from a system subjected to damping forces.

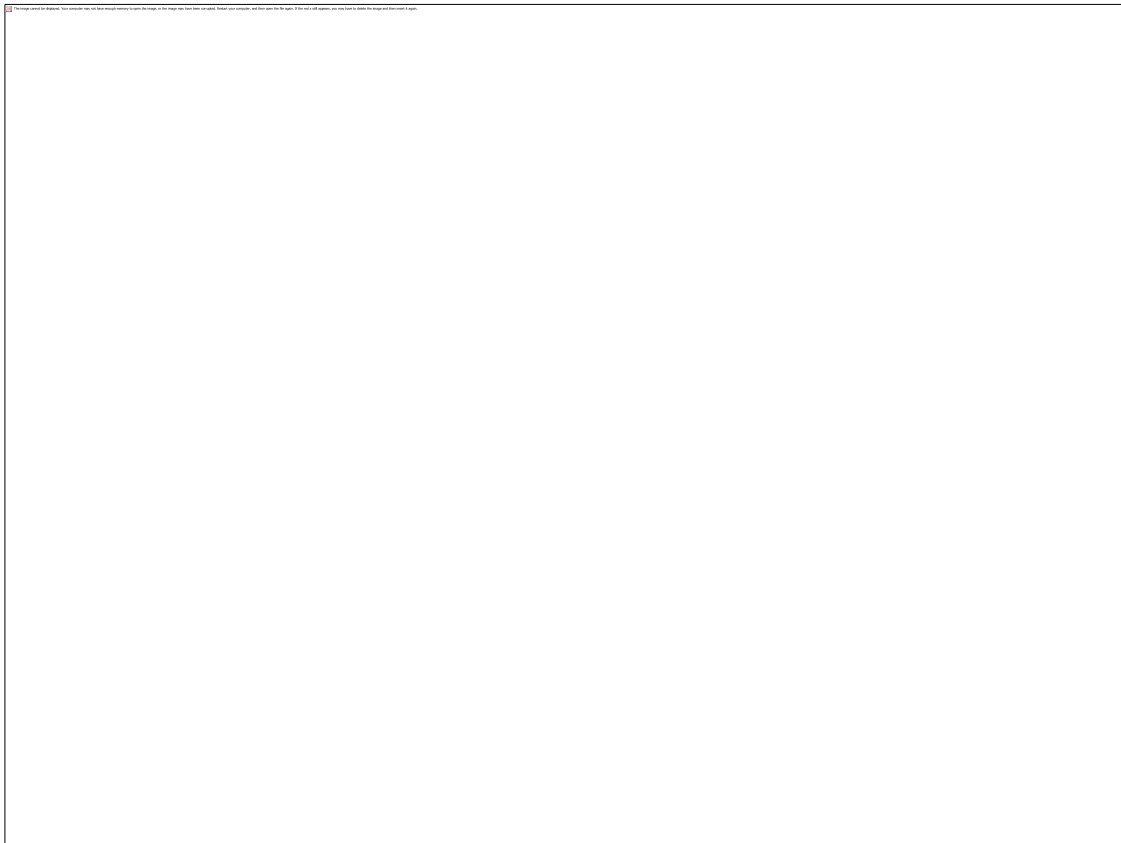


Figure 13: Displacement vs Time (Bottom)

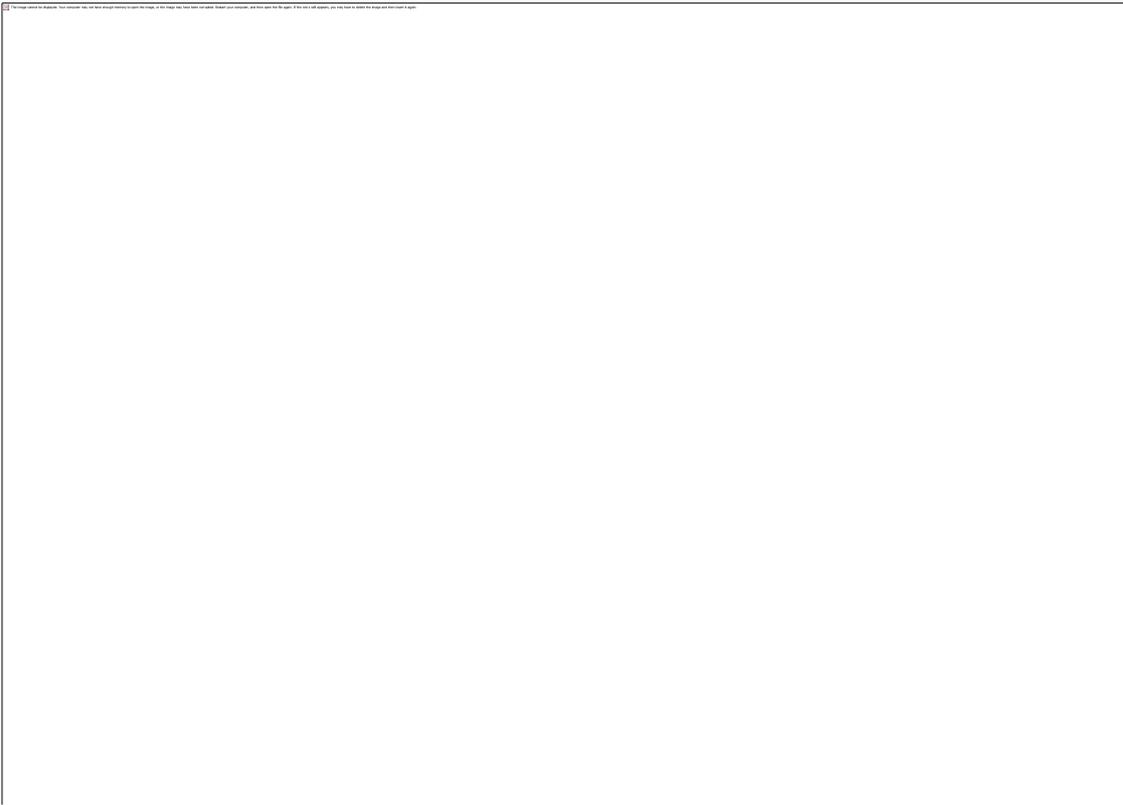


Figure 14: velocity vs Time (Bottom)

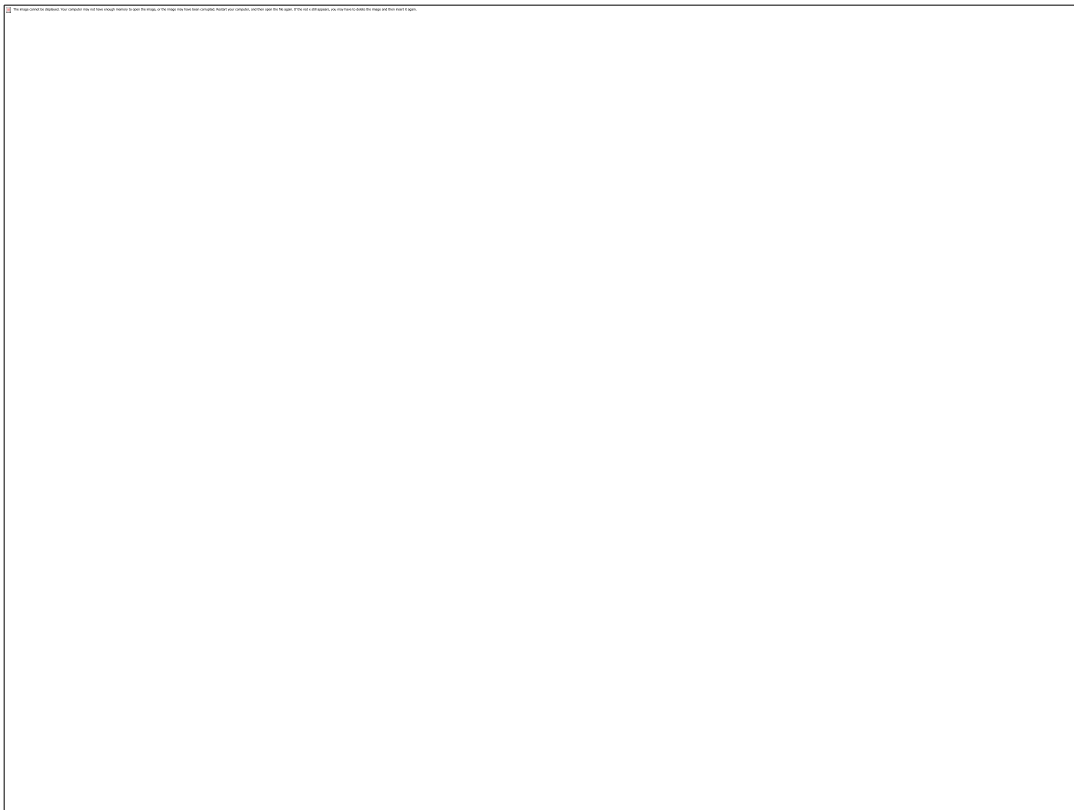


Figure 15: Acceleration vs Time (Bottom)

3.3.3 Bottom Section Dynamics: The bottom section of the riser displays unique characteristics distinct from

the top and middle sections. The displacement graph reveals an initial sharp peak, indicative of a sudden force or excitation impacting the riser. This is followed by oscillatory behavior that diminishes over time, reflecting the natural response of the riser to dynamic loading. The final state of the graph suggests that the riser settles into a tension-dominated state after experiencing dynamic excitation, approaching a constant displacement. In terms of velocity, the bottom section also shows a rapid initial response with significant peaks and subsequent damped oscillations, reflecting the pronounced influence of external forces acting at this location. By the end of the observation period, the velocity stabilizes, suggesting that the motion of the riser near the wellhead is approaching equilibrium. The acceleration profile for the bottom section is marked by a significant negative spike followed by a positive peak, illustrating the strong forces acting on the riser at its base. This section experiences sharper and more aggressive oscillations compared to the middle segment, likely due to proximity to the seabed, where higher reaction forces and damping effects occur. Overall, the analysis of displacement, velocity, and acceleration across the riser's sections demonstrates the complex dynamic interactions experienced by the riser under varying conditions, providing critical insights for future design and operational considerations in deep-water environments.

3.4 Corrosion results

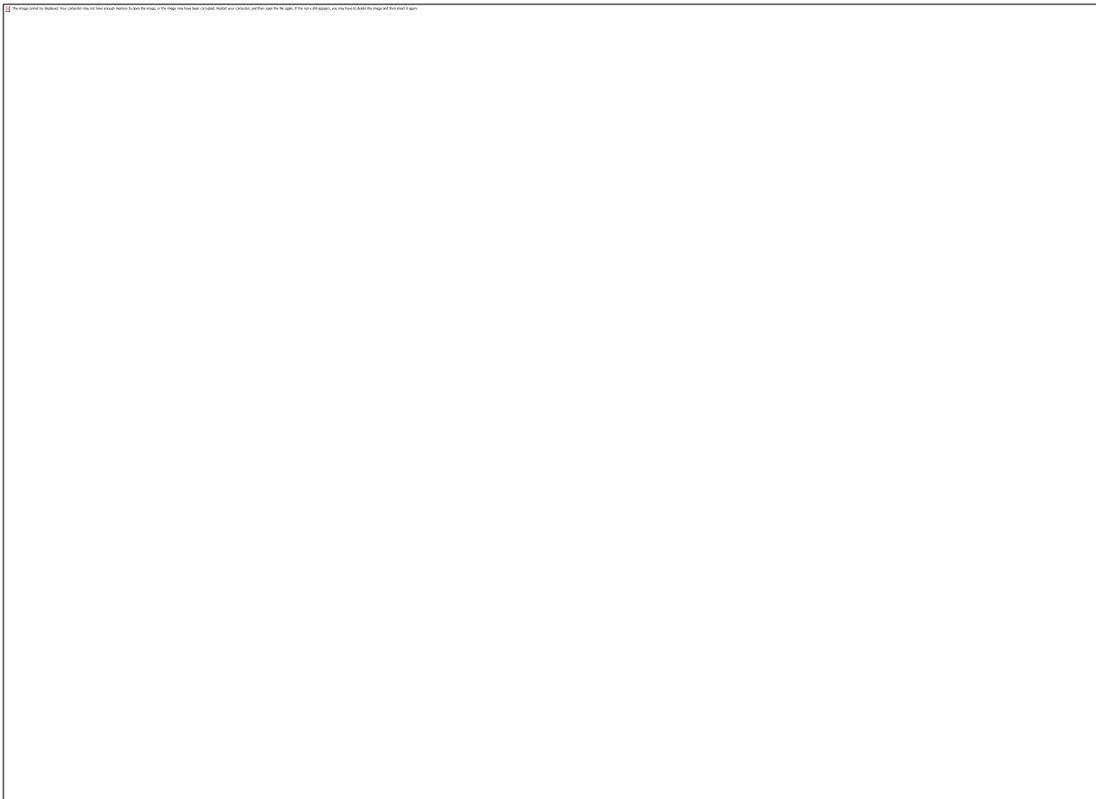


Figure 16: Corrosion rate with respect to velocity and with respect to pressure

3.4.1 Corrosion Analysis of the Riser

The corrosion analysis focuses on external and internal mechanisms, primarily driven by electrochemical reactions, flow velocity, and pressure.

External Corrosion: Influenced by electrochemical reactions modeled by Faraday's Law, external corrosion is a critical factor in long-term riser degradation. The rate of corrosion is influenced by environmental factors, which affect the riser's surface through anodic and cathodic reactions .

Internal Corrosion: The analysis identifies two main factors: diffusion and erosion. Erosion corrosion, driven by high fluid velocity and pressure, accelerates the degradation of the riser's internal material. In high-velocity

flow environments, the combined effects of mechanical wear and chemical attack cause material loss. The influence of velocity and pressure is analyzed through two graphs that emphasize their significant impact.

Velocity vs. Corrosion Rate: The graph demonstrates a non-linear, exponential relationship between fluid velocity and corrosion rate. As velocity increases, particularly beyond 6 m/s, the corrosion rate rises sharply, indicating that small increases in flow velocity can result in disproportionately large corrosion rates. This suggests that managing fluid velocity is essential to mitigate internal corrosion in the riser .

Pressure vs. Corrosion Rate: Similarly, the pressure graph reveals an exponential growth in corrosion rate with increasing pressure. The rise in corrosion is particularly evident in the range of 1×10^7 Pa to 2×10^7 Pa, where corrosion rates steeply increase. This underscores the importance of pressure control in minimizing internal corrosion, particularly in high-pressure riser environments such as deepwater systems

Both internal and external corrosion mechanisms emphasize the critical need for corrosion control strategies in the design and operation of risers, especially in high-pressure, high-velocity environments common in subsea pipelines.

3.5 Result validation

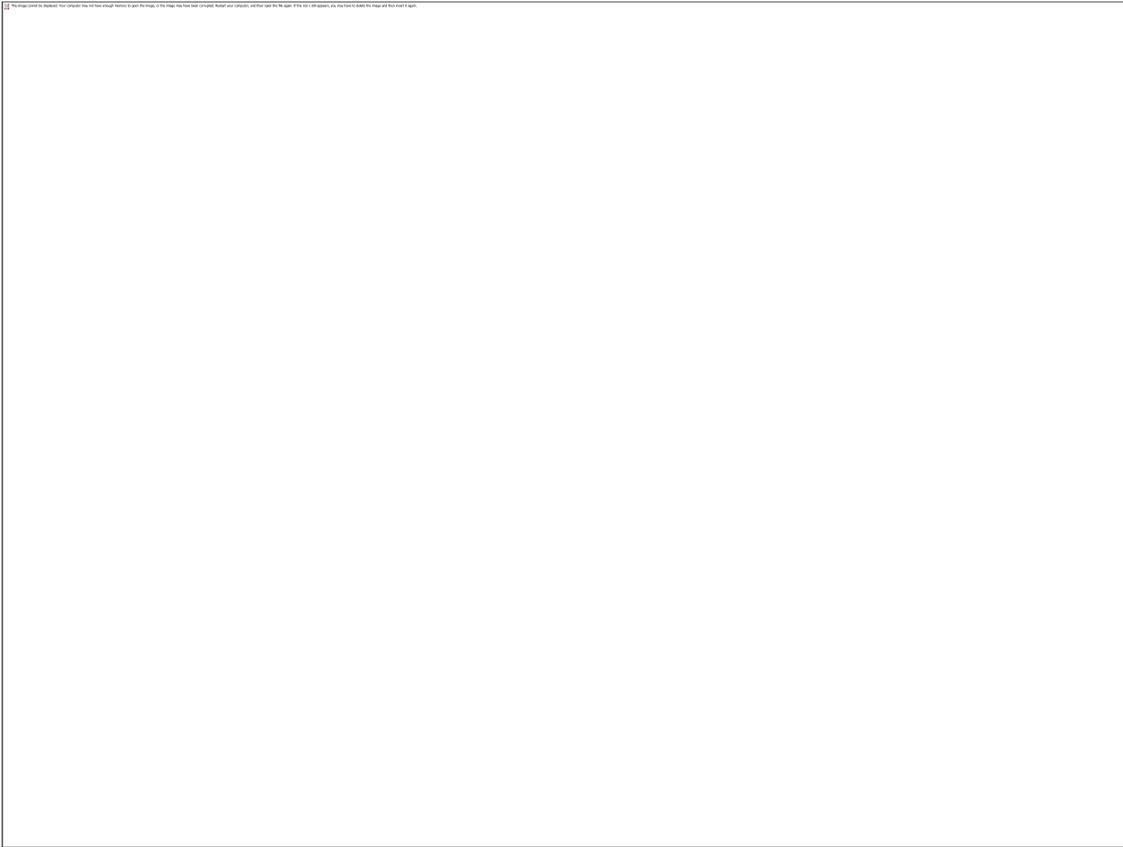


Figure 17: Riser validation

3.5.1 Result Validation

The validation of the structural dynamics of a Lazy Wave Riser was conducted by comparing simulation results from the MATLAB-based tool "RiSat" with the established software OrcaFlex. Both tools exhibit a consistent downward trend in tension profiles along the riser's arc length, reflecting the expected behavior as effective tension decreases from the top toward the seabed due to the effects of weight and hydrostatic forces. Importantly, both models accurately capture the transition from tensile to compressive forces around the mid-length of the riser, confirming their validity in simulating riser dynamics.

Despite the overall agreement, some discrepancies were observed. In the initial section (0–500 m), OrcaFlex predicted slightly higher initial tensions, likely due to differences in buoyancy treatment. The middle section (1000–2000 m) showed a divergence, with OrcaFlex consistently reporting higher tensions, which may be influenced by varying material properties and loading conditions. However, both models converged again in the lower section (2500–3000 m), indicating consistency in modeling the transition to compressive forces at the seabed. This validation reinforces the reliability of RiSat for further subsea engineering analyses.

IV.DISCUSSION AND CONCLUSION

This study presents a comprehensive analysis of the static and dynamic behavior of a Lazy Wave Riser using the MATLAB-based tool "RiSat." The static analysis revealed critical trends in tension, bending moment, and shear force along the riser, highlighting the importance of understanding these parameters in managing offshore riser systems. The tension profile exhibited a decrease from the top to the bottom of the riser, reflecting the effects of weight and hydrostatic forces, while bending moments stabilized beyond a certain depth, indicating a more uniform force distribution. The modal analysis identified six natural vibration modes, illustrating the dynamic response of the riser to external loading. Notably, low-frequency oscillations with increasingly complex deformation patterns were observed, emphasizing the potential for fatigue risks and the importance of dynamic design considerations in offshore applications.

Dynamic analysis at different riser sections revealed significant variations in displacement, velocity, and acceleration, underscoring the complex interactions experienced by the riser under varying conditions. The top section demonstrated pronounced oscillatory behavior, while the middle section exhibited more stable dynamics, suggesting differing influences of external forces along the riser length. The bottom section showed rapid initial responses and higher oscillations, reflecting the significant impact of seabed interactions.

Furthermore, the corrosion analysis indicated critical insights into both internal and external mechanisms affecting the riser's integrity. The correlation between flow velocity, pressure, and corrosion rates highlights the necessity for robust corrosion control strategies, particularly in high-pressure and high-velocity environments typical of subsea pipelines. The validation of the RiSat tool against OrcaFlex confirms the reliability of the simulation results, with both models exhibiting consistent tension profiles along the riser. Discrepancies noted in certain sections underscore the complexity of modeling riser dynamics, necessitating further refinement of computational approaches.

In conclusion, this research contributes valuable insights into the structural dynamics of Lazy Wave Risers, offering essential information for engineers and designers in the subsea industry. Future studies should focus on refining modeling techniques and exploring advanced materials and coatings to mitigate corrosion risks, ultimately enhancing the performance and longevity of offshore riser systems.

REFERENCES

- [1]. Audoly, B. and Pomeau, Y. (2010) Elasticity and Geometry: from Hair Curls to the Non-linear Response of Shells. Oxford University Press, USA.
- [2]. Chung, J. (1982) Hydrodynamic Forces on a Marine Riser: A Velocity-Potential Method. *Journal of Energy Resources Technology*, 104(54), 53 – 57.
- [3]. Guo, B., Song, S., Ghalambor, A. and Lin, T. (2014) Offshore pipelines: design, installation, and maintenance. In: Engineering Professional Collection, second ed. Elsevier Science, Boston, USA.
- [4]. Levenberg, K. (1944) A Method for the Solution of Certain Problems in Least-Squares, *Quarterly Applied Mathematics* 2(1), 164-168.
- [5]. Liu, X., Sun, H., Li, Y., Chang, Y., Liu, K., Chen, G., Sheng, L., & Xu, L. (2022). Theoretical modeling and analysis for mechanical properties of deepwater workover riser system. *Ocean Engineering*, 257, 111701. <https://doi.org/10.1016/j.oceaneng.2022.111701>.
- [6]. Mark, J. (2019). Decommissioning forecasting and operating cost estimation. *Science Direct Journal*, 2019(10), 207 - 223.
- [7]. Mathworks(2023) Solve System for Non-linear Equations. The mathworks website, <https://www.mathworks.com/help/optim/ug/fsolve.html>. Accessed: 02:30 PM 12th July, 2024.
- [8]. Morison, J., O'Brein, M., Johnson, J. and Schaaf, S. (1950) The force exerted by surface waves on piles. *Journal of The American Institute of Mining, Metallurgical, and Petroleum Engineers*, 189, 149–154. <https://doi.org/10.2118/950149-G>.
- [9]. Nestor, P. (2004) Electrochemistry and corrosion science. Kluwer Academic Publishers. Boston, USA.
- [10]. Ning, J. & Jinkun, L. (2022) Boundary Control of Flexible Three-Dimensional Euler–Bernoulli Beams. Springer, Singapore.
- [11]. NS Energy (2019) Navigating the challenges of subsea oil and gas equipment installation. NS Energy website: <https://www.nsenerybusiness.com/features/subsea-oil-gas-installation/> accessed 12:45 am, 25 June, 2023.
- [12]. Obaseki, M., Alfred, P., Elijah, P., and Okuma, S. (2023) Corrosion Rate Prediction in Oil and Gas Pipelines Based on Multiphase Flow Modelling. *International Journal of Engineering Research in Africa*, 1(16) 27-48
- [13]. Oil and gas portal (2015) Oil and gas subsea | subsea technology and equipment. Oil and gas portal website: <https://www.oil-gasportal.com/subsea-technology-and-equipment/> accessed 1:15 am, 28 June, 2023.
- [14]. Qiao, H., Ruan, W., Shang, Z., and Bai, Y., (2016) Non-Linear Static Analysis of 2D Steep Wave Riser under Current Load. Proceedings of the ASME 2016 35th International Conference on Ocean, Offshore and Arctic Engineering, Busan, South Korea.
- [15]. Randolph, M. and Gourvenec, S. (2011) Offshore Geotechnical Engineering. Taylor & Francis. USA.
- [16]. Reddy, J. (2015) An Introduction to Nonlinear Finite Element Analysis: with Applications to Heat Transfer, Fluid Mechanics, and Solid Mechanics. Oxford University Press, USA
- [17]. Rivero-Angeles, F., Vázquez-Hernández, A., and Martínez, U. (2014) Vibration analysis for the determination of modal parameters of steel catenary risers based on response-only data. *Journals of Engineering Structures*, 59 (2014) 68-79.
- [18]. Tian, D., Fan, H., Leira, B., Sævik, S., & Fu, P. (2020). Static analysis of interaction between two adjacent top tensioned risers with consideration of wake effects. *Ocean Engineering*, 195(2020), 106-116. <https://doi.org/10.1016/j.oceaneng.2019.106662>
- [19]. Tapper, P. (2020) Feasible numerical analysis of steel lazy-wave riser. *Journal of Ocean Engineering*, 195 (2020) 10098- 10115.
- [20]. Wang, J., Duan, M., He, T., Jing, C. (2014) Numerical solutions for nonlinear large deformation behaviour of deepwater steel lazy-wave riser. *Ships Offshore Struct.* 9, 655–668. <https://doi.org/10.1080/17445302.2013.868622>.
- [21]. Yong, B., & Qiang, B. (2005). *Subsea pipelines and risers*. Houston, USA: Elsevier.
- [22]. Yong, B., & Qiang, B. (2010). *Subsea Engineering Handbook*. Houston, USA: Elsevier